DEVELOPMENT OF A SEMI-AUTOMATIC ALGORITHM FOR DECONVOLUTION AND QUANTIFICATION OF THREE-DIMENSIONAL MICROSCOPY IMAGES

N. B. Vicente, J. E. Diaz-Zamboni, J. F. Adur, M. F. Izaguirre, C. D. Galetto, V. H. Casco*

Laboratorio de Microscopia Aplicada a Estudios Moleculares y Celulares. Facultad de Ingeniería, Universidad Nacional de Entre Ríos (UNER). Ruta 11, Km. 10 (3101) Oro Verde, Entre Ríos, Argentina.

*Corresponding author, E-mail: vcasco@bioingenieria.edu.ar

Recibido: Marzo 2010. Aprobado: Septiembre 2010.
Publicado: Noviembre 2010.

ABSTRACT

Modern microscopy enables the acquisition of massive volumes of information. Processing and evaluating large multidimensional images is time-consuming, especially when working with various stacks. In the present work we have developed a software tool for the optimization of image processing, which consists of an automatic deconvolution and quantification algorithm that eliminates non-systematic errors and significantly decreases processing time. This tool included a restoration deconvolution method (positive constrained algorithm) and five image-restoration parameters (Contrast-to-Noise Ratio, Signal-to-Noise Ratio, Full-Width at Half-Maximum and two three-dimensional Tenengrad-based indicators) used to assess quantitatively the quality of restoration. This algorithm was used to process raw three-dimensional images using several experimental Point Spread Functions; raw images were obtained by fluorescence wide-field microscopy of epidermal E-cadherin expression in *Rhinella (= Bufo) arenarum* embryos and fluorescent microspheres. The image-restoration indicators and the performance of the algorithm were evaluated. Results show that all indicators concur and do not increase processing time significantly, constituting a valuable tool for 3D microscopy analysis.

Keywords: Automatic algorithm; deconvolution; quantification; microscopy; multidimensional images.

DESARROLLO DE UN ALGORITMO SEMI-AUTOMATICO PARA DESCONVOLUCIONAR Y CUANTIFICAR IMAGENES DE MICROSCOPIA TRIDIMENSIONAL

RESUMEN

La microscopía moderna permite la adquisición de volúmenes masivos de información. El procesamiento y evaluación de grandes imágenes multidimensionales consumen gran cantidad de tiempo, especialmente cuando se trabaja con varios apilamientos. En el presente trabajo hemos desarrollado un software para la optimización del procesamiento de imágenes multidimensionales que elimina los errores no-sistemáticos y disminuye el tiempo de procesamiento. Éste consiste en un algoritmo automático de desconvolución de restauración (desconvolución con restricción de positividad) y cinco indicadores de restauración de imágenes (Ancho Total a la Mitad del Máximo, Relación Contraste-Ruido, Relación Señal-Ruido y dos indicadores tridimensionales basados en la función Tenengrad) usados para evaluar cuantitativamente la calidad de restauración. Este algoritmo fue utilizado para procesar imágenes tridimensionales utilizando diversas Funciones de Esparcimiento Puntual experimentales; las imágenes se obtuvieron mediante microscopia de fluorescencia de campo amplio del patrón de expresión de E-cadherina en piel de embriones de *Rhinella (=Bufo) arenarum* y de microesferas fluorescentes. Se evaluaron los indicadores de restauración y el rendimiento del algoritmo. Los resultados muestran que los indicadores concuerdan y no incrementan significativamente el tiempo de procesamiento, constituyendo una valiosa herramienta para el análisis de microscopia 3D.

Palabras claves: algoritmo automático, desconvolución, cuantificación, microscopia, imágenes multidimensionales.

INTRODUCTION

The microscope's image formation process is modeled by (1), where (x,y,z) are spatial coordinates, $i(x,y,z)$ is the raw image which is formed by the three-dimensional (3D) convolution (denoted by $\otimes$) of the original object $o(x,y,z)$ and the system's transfer function, denominated Point Spread Function, $PSF(x,y,z)$ [1].

$$i(x,y,z) = o(x,y,z) \otimes PSF(x,y,z) \quad (1)$$

In digital deconvolution microscopy, raw multidimensional images are deconvolved to produce images which resemble the original object more closely [2]. Briefly, this procedure attempts to reverse the modifications brought about by the PSF and in order to accomplish this task a theoretical or experimental PSF is required. The positive constrained iterative deconvolution method is a restoration algorithm [3] which works in the following manner. First, an estimation of the original object is proposed. Then, the estimate is convolved with an adequate PSF and the resulting image is compared to the raw one, producing correction factors which are used to improve the estimation while ensuring it contains only non-negative values. This process continues until certain exit criteria are met. Several variables may be evaluated in order to assess the quality of restoration after deconvolution [4] [5]. These may be general (such as Contrast-to-Noise Ratio, CNR, Signal-to-Noise Ratio, SNR, and Tenengrad-based indicators) or for a specific specimen (for instance, the Full-Width at Half-Maximum parameter, FWHM, for spherical objects) [6]. CNR and SNR values are calculated using (2) and (3), respectively.

$$\mathrm{CNR} = 20\log\left(\frac{\text{Dynamic range of the signal}}{\text{Standard deviation of the noise}}\right) \quad (2)$$

$$\mathrm{SNR} = 20\log\left(\frac{\text{Mean intensity of the signal}}{\text{Standard deviation of the noise}}\right) \quad (3)$$

The Tenengrad function shown in (4) provides a value that indicates the degree of focusing of a given 2D image [7] [8], where *Ix* and *Iy* are gradient images which result from the convolution of the original image with the sobel operators [1]. In order to work with 3D images, we propose two 3D Tenengrad-based indicators which are shown in (5) and (6).

$$\mathrm{Tenengrad} = \sum_{i=1}^{X}\sum_{j=1}^{Y}\left(I_x^2(i,j) + I_y^2(i,j)\right) \quad (4)$$

$$\mathrm{TEN} = \max_z\left[\sum_{i=1}^{X}\sum_{j=1}^{Y}\left(I_x^2(i,j) + I_y^2(i,j)\right)\right] \quad (5)$$

$$\mathrm{TENr} = \max_z\left[\sum_{i=1}^{X}\sum_{j=1}^{Y}\sqrt{I_x^2(i,j) + I_y^2(i,j)}\right] \quad (6)$$

Since deconvolution enhances high-frequency areas at the expense of low-frequency zones (process modulated by the PSF), deconvolved images have more contrast than their corresponding raw ones, and therefore have higher CNR values. Moreover, deconvolution assigns out-of-focus fluorescence to its correct spatial position; this procedure reduces noise (resulting in higher SNR values) and increases the degree of focus (evidenced by higher TEN and TENr values).

As an example, figure 1 shows CNR, SNR, TEN and TENr values of a raw 2D image (1b) which was sharpened with an unsharp contrast enhancement filter (process equivalent to deconvolution; 1a) and smoothened with a Gaussian low pass filter (procedure comparable to a convolution with a PSF; 1c).

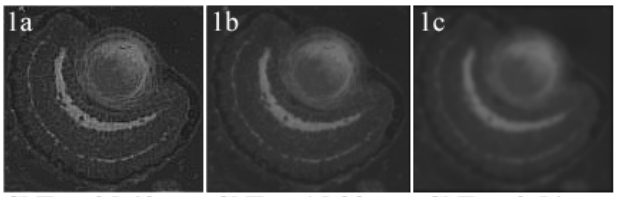

Fig. 1. CNR, SNR, TEN and TENr values of the raw image after an unsharp contrast enhancement filter was applied (1a), the original raw image (1b) and the raw image after it was smoothened with a Gaussian low pass filter (1c). Images show the total NCAM expression pattern in retinal tissue of *Rhinella (=Bufo) arenarum* tapdoles.

The FWHM parameter can be used to measure the diameter of spherical objects such as microspheres. Steps involved in the calculation of the FWHM are as follows. First, an intensity profile is obtained from a path traced through the object's center point. Then, the maximum intensity value *I* is determined and the distance between

the two points that correspond to an intensity equal to *I*/2 is provided as the FWHM; this value corresponds to the object's diameter.

In the present work an existing processing algorithm which automatically deconvolved raw images and evaluated image sets after deconvolution was enhanced. Two new image-restoration indicators were added in the form of uncoupled modules to an existing structure which included a restoration deconvolution algorithm (positive constrained iterative method) and three quantification methods (CNR, SNR and FWHM). Given that FWHM, CNR and SNR indicators have been previously implemented and assessed [9], TEN and TENr parameters will be evaluated in the present work; moreover, the performance of both versions of the algorithm will be compared. The improved algorithm was implemented in calculus software (Matlab v7.0) and was used to process each of four different raw 3D images with thirty PSFs obtained under diverse experimental conditions (five samples of each condition were selected for statistical purposes).

MATERIALS AND METHODS

The processing algorithm was implemented in calculus software in a personal computer (Intel Pentium IV 1.81 GHz with 1 GB of RAM and 230 GB of hard-disc space). Raw images were obtained by optical-sectioning [10] using an Olympus BX50 upright microscope, equipped with a white-light source for transmitted microscopy and a mercury UV-lamp for epi-fluorescence microscopy. Images were taken with a cooled monochromatic Apogee CCD camera of 14 bits of resolution, 768 x 512 pixel^2 sensor size, 9x9 μm^2 pixel size, mounted to the microscope by a mount C lens (0.5X). A stepping motor (RS 440-436) attached to the fine adjustment knob of the microscope enabled the displacement of the stage up and down in steps of multiples of 5 nm [11]; it was controlled via parallel port by a personal computer with an Intel Pentium II 350 MHz processor, 256 MB of RAM and 6 GB of hard-disc space. Images were transferred through Ethernet to the computer in which the processing algorithm was executed.

The CCD camera and stepping motor were controlled by a special software which also included deconvolution algorithms [12] and a 3D visualization interface; it was designed in Object Pascal language [13]. Optical sectioning was automatically done by this tool after loading some basic parameters which included image dimensions, time of exposure, distance between in-focus planes and motor speed (which determined stage speed). Images were saved in TIFF 8 bit format and stacks were visualized with the aid of an algorithm which enabled Maximum Intensity Projection (MIP), implemented in OpenGL.

Optical Sectioning

The work-area was selected using a low magnification lens and white light (transmitted) which does not excite the fluorophore and therefore prevents photobleaching [14][15][16]. When switching to UV illumination, the micrometric screw was adjusted to focus using either a 40X (NA 0.85, determining voxels of 0.45x0.45x0.5 μm^3) or 100X objective lens (NA 1.35, 0.18x0.18x0.25 μm^3 voxel size). Then, the stage was moved upwards a distance equal to half the total depth of the future stack and the stepping motor was programmed to move it downwards in step of 0.5 or 0.25 μm (for 40X and 100X, respectively). The final stack size ranged between 128x128x64 and 256x256x256 pixels^3.

Positive Constrained Deconvolution Method

Figure 2 shows a flowchart of the deconvolution algorithm's sequence. After variable initialization, a normalized PSF is selected and an estimation of the original object is proposed (in this case, the normalized raw image was employed). Then, the Fast Fourier Transform (FFT) is applied to both volumes (transforming them into Fourier space) and their module are multiplied pixel-wise (procedure equivalent to a

convolution in Real space). The resulting volume is anti-transformed by the inverse FFT (iFFT) and after being compared to the raw image, a new estimation is produced. A non-negativity constraint is imposed on the new estimate since the signal's dynamic range is made up of non-negative values only. This process continues until certain exit criteria are met; in this case, such criteria consisted of a convergence criterion (which was met when the maximum difference *e* between the estimation and the raw image was no longer significant, that is to say, $e < 1/255$) and a maximum-iteration limitation (establishing that deconvolution cycles would not surpass ten iterations).

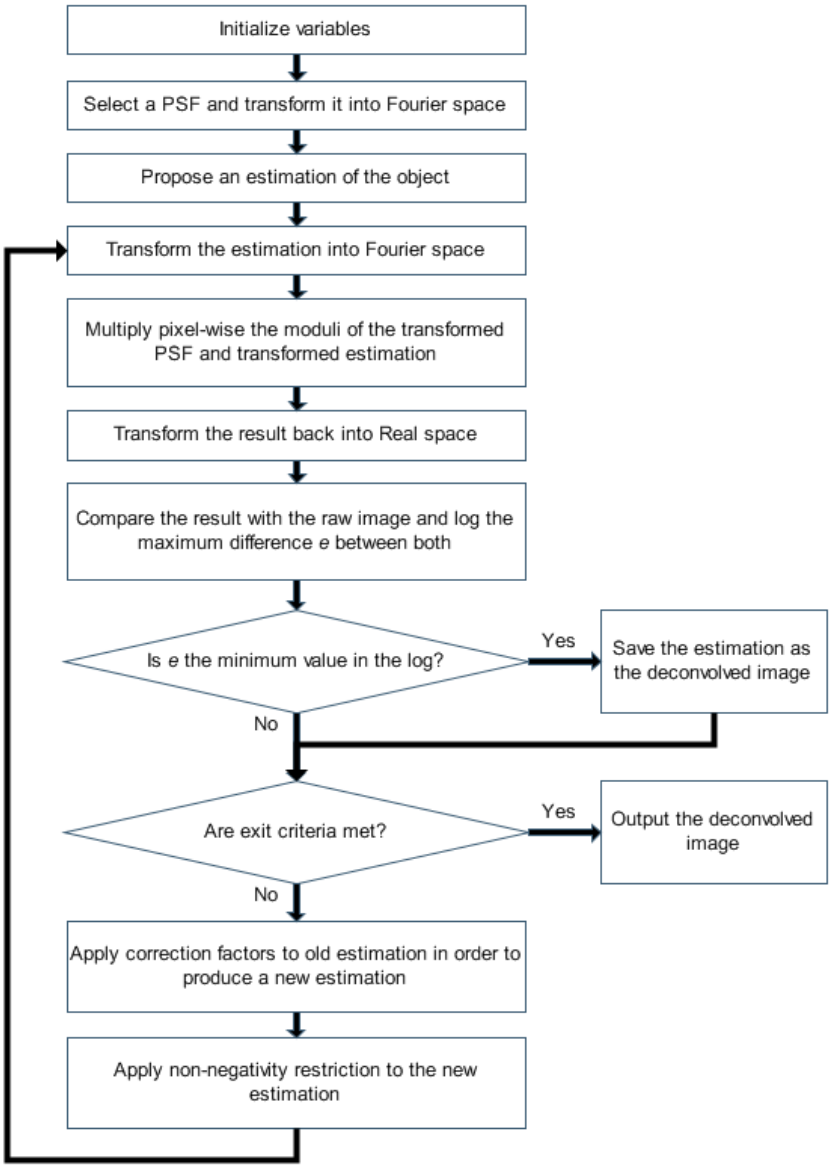

Fig. 2. Steps involved in the positive constrained deconvolution algorithm.

Quantification Methods

Two general image-quality indicators (TEN and TENr) and a specimen-specific parameter (FWHM) were used to assess the quality of restoration after deconvolution. TEN and TENr were used to evaluate images of epidermal E-cadherin expression in *Rhinella arenarum*

embryos, while the FWHM parameter was employed to calculate the diameter of fluorescent microspheres along the x, y and z axis [9].

PSF Preparation

Fluorescent microspheres (F-8888 kit; Molecular Probes, OR, USA) were used as point-sources of light to produce PSFs under thirty different experimental conditions (five samples of each condition were selected for statistical purposes). These microspheres were selected according to size so that the Nyquist criterion was satisfied [17]. Consequently, fluorescent beads which were 0.18 and 0.46 μm in diameter were selected for the 40X objective lens, while 0.11-μm and 0.18-μm microspheres were used for the 100X objective lens.

Table I. Experimental conditions under which PSFs were obtained; ideal conditions are marked with an asterisk (*) [9].

Parameter	40X	100X
Coverslips type (thickness in μm)	0 (80-120)	
	1 (130-160)	
	1.5 (160-190) *	
	2 (190-220)	
Correction-collar value	0.11	-
	0.14	-
	0.17 *	-
	0.20	-
	0.23	-
Mounting medium (refractive index)	Air (1)	
	Water (1.33)	
	Vectashield (1.46)	
	Glycerol [1] (1.47)	
	Oil [2] (1.51) *	
Numerical aperture	-	0.5
	-	1.0
	-	1.35 *
Immersion medium (refractive index)	-	Air (1)
	-	Water (1.33)
	-	Glycerol [1] (1.47)
	-	Oil [2] (1.51) *

[1] Glycerol: Cicarelli, San Lorenzo, Santa Fe, Argentina.

[2] Oil: Olympus, America Inc., Buenos Aires, Argentina.

Original solutions containing 0.11-μm, 0.18-μm and 0.46-μm fluorescent microspheres were diluted in distilled water (1:100) and a 5 μL drop of each was placed on a coverslip and left aside until dehydration. Then, these coverslips were placer over slides containing a drop of mounting media. When using the 100X lens, a drop of immersion medium was placed on top of the coverslip. Table I summarizes the thirty experimental conditions which were evaluated.

Specimen Preparation

Two types of specimens were imaged: 4-μm fluorescent microspheres and *Rhinella arenarum* whole embryos incubated with IgG-FITC-anti-E-cadherin. One sample of each specimen was used per objective lens and per PSF-microsphere size, totaling eight 3D raw images.

Fluorescent Microspheres

4-μm fluorescent microspheres were prepared according to the PSF-preparation protocol explained in the previous section, using the ideal condition (see Table I).

Rhinella arenarum Embryos

Stage-19 (Gosner, 1960 [18]) *Rhinella arenarum* embryos were treated to study the skin cell-adhesion-molecule E-cadherin [19][20] expression pattern following Larrea's protocols [21][22]. They were fixed in Carnoy, washed in 1X PBS at room temperature and then treated with Triton X-100 (SIGMA Chemical Company, St. Louis, USA) 0.1% in PBS during 30 minutes at room temperature. They were then incubated in goat normal serum 1:20 for 35 minutes followed by anti-E-cadherin antibody (mouse monoclonal antibody; Transduction Laboratories, Lexintong USA) 1:50 at 37°C for 75 minutes. Next, embryos were washed in 1X PBS and incubated with the IgG-FITC (SIGMA) 1:64 at room temperature for 105 minutes and then washed again with 1X PBS; finally, they were mounted in Vectashield mounting medium (Vector Laboratories, Vector Burlingame, CA) to prevent fluorescent decay.

RESULTS AND DISCUSSION

Raw images of fluorescent microspheres exhibit an elongated diameter along the z axis which is reduced by deconvolution (Fig. 3). Figure 4 shows this phenomenon for fluorescent microspheres imaged with the 40X objective lens, which were deconvolved with PSFs obtained using diverse mounting media (Table 1). This bar graph evidences that z-elongation reduction depends on the PSF employed in the deconvolution process. Moreover, it shows that the closer a PSF is to the ideal transfer function, the greater the reduction.

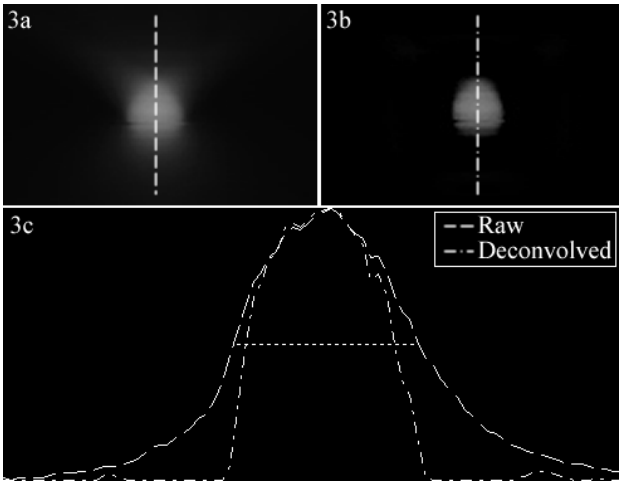

Fig. 3. Images show *xz* projections of a raw 4-µm fluorescent microsphere (3a) and the same microsphere after deconvolution with an ideal PSF (3b). Intensity profiles (3c) were traced along paths parallel to the z axis. The dotted line indicates where the FWHM is measured for both curves.

As expected, the values of all image-restoration indicators (CNR, SNR, TEN and TENr) are higher for deconvolved images than for the corresponding raw ones (Fig. 5 and 6). Furthermore, these values increase as PSF conditions approach ideal ones. TEN and TENr bar graphs (Fig. 6) present greater differences between the diverse experimental conditions than CNR and SNR graphs (Fig. 5) for the same *Rhinella arenarum* skin images.

Time is an important factor that must be taken into consideration when working with large volumes of information. A comparison table showing the time taken to process all raw images with the previous and enhanced versions of the processing algorithm is shown in Table II.

Table II: Time taken to apply the previous and enhanced versions of the processing algorithm to all raw images.

Specimen	Image size (pixels)	Processing time	
		Previous version	Enhanced version
Fluorescent microsphere	256x256x64	73 min	73 min
	128x128x64	64 min	64 min
Epidermal E-cadherin expression pattern	128x128x128	127 min	121 min
	128x128x256	138 min	141 min

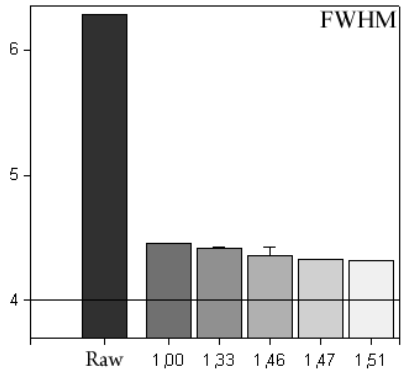

Fig. 4. FWHM values for fluorescent microspheres imaged with the 40X objective lens, which were deconvolved with PSFs obtained using 0.46-µm fluorescent microspheres and different mounting media. The horizontal line represents the real microsphere diameter (4 µm).

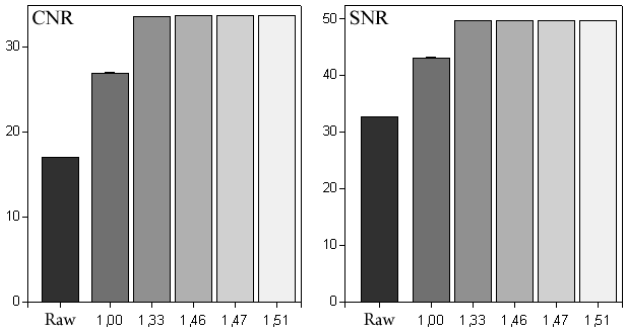

Fig. 5. CNR and SNR values for epidermal E-cadherin expression in *Rhinella arenarum* embryos imaged with the 40X objective lens, which were deconvolved with PSFs obtained using 0.46-µm fluorescent microspheres and different mounting media.

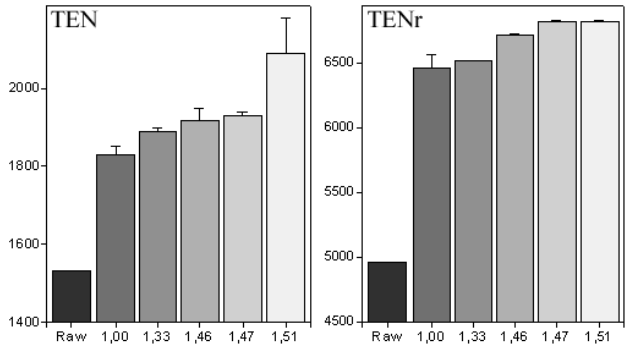

Fig. 6. TEN and TENr values for epidermal E-cadherin expression in *Rhinella arenarum* embryos imaged with the 40X objective lens, which were deconvolved with PSFs obtained using 0.46-µm fluorescent microspheres and different mounting media.

In the present work, an existing processing algorithm for digital deconvolution microscopy was enhanced by the addition of two new image-restoration indicators (TEN and TENr). Results obtained with these indicators are concordant with previously obtained results using CNR, SNR and FWHM parameters [9]. These have demonstrated that deconvolution is sensitive to variations in the PSF and that the best restoration results are achieved when the PSF employed is obtained under conditions similar to the ideal ones (Fig. 4 through 6).

Both versions of the automatic algorithm convey a significant reduction in processing time (Table II). It took under seven hours to complete the image processing task, that is to say, to deconvolve each of four raw 3D images with a hundred and fifty different PSFs (thirty experimental conditions, n = 5), totaling 600 different deconvolution processes, followed by the evaluation of the resulting deconvolved images with at least one of five image-restoration quantification methods. If the same task was carried out manually, it would take an operator days or even weeks. Furthermore, the processing time of both versions of the algorithm differ in less than 5%; we can therefore conclude that the new modules do not reduce the algorithm's performance.

In order to perform an accurate quantification, a restoration deconvolution method was selected since deblurring tools eliminate potentially-useful information. Other deconvolution and quantification methods may be added or may replace the present ones with minor adjustments to the code due to the uncoupled-module design of the processing algorithm. Methods contained in new modules should ensure that data is not lost during processing because an incorrect treatment of the samples will lead to inappropriate quantitative analyses. Additionally, the algorithm is an unbiased method of evaluation which eliminates non-systematic errors in the quantification process since it is independent of the operator.

CONCLUSIONS

The present algorithm is readily applied to multidimensional images produced by other techniques such as transmitted-light and confocal microscopy. Furthermore, other image formats (such as JPEG, BMP, GIF and PNG) are currently supported in addition to the TIFF files employed in the present work.

In future works we plan to continue improving the present algorithm by the addition of new modules. We plan to implement other quantification methods to assess image restoration after deconvolution, such as sharpness indicators which may include the normalized variation parameters; also, new deconvolution methods might be added to the algorithm (for instance, a blind deconvolution method). Moreover, a new version of the mentioned algorithm may be programmed using an object-based language (such as C++) so as to provide microscopy users with standalone software with a user-friendly interface.

ACKNOWLEDGEMENTS

This work was supported by grants from SCYTFRH-UNER, PID 6082–1 (to V.H.C.) and PID 6088–1 (to M.F.I.).

REFERENCES

[1] Castleman K.R. *Digital Image Processing*. Prentice Hall, New Jersey, 1996.

[2] Sarder P., Nehorai A. (2006) "Deconvolution methods for 3-D fluorescence microscopy images". *IEEE Signal Processing Magazine* 23:32-45

[3] Wallace W., Schaefer L.H., Swedlow J.R. (2001) "A workingperson's guide to deconvolution in light microscopy". *Biotechniques* 31:1076-1097

[4] Grgic S., Grgic M., Mrak M. (2004) "Reliability of objective picture quality measures". *Journal of Electrical Engineering* 55:3-10

[5] Yao Y., Abidi B.R., Abidi M.A. (2007) "Extreme Zoom Surveillance: System Design and Image Restoration". *Journal of Multimedia* 2:20-31

[6] Adur J.F. (2006) "Determinación de las propiedades ópticas de un sistema de epifluorescencia y su utilización en estudios de microscopía cuantitativa de 3D". *Biomedical Engineer Magister Thesis*, Faculty of Engineering – Bioengineering. Entre Ríos National University. Argentina

[7] Conchello J.A., Lichtman J.W. (2005) "Optical sectioning microscopy". *Nature Methods* 2:920-931

[8] Santos A., Ortiz de Solórzano C., Vaquero J.J., Peña J.M., Mapica N., Del Pozo F. (1997) "Evaluation of autofocus functions in molecular cytogenetic analysis". *Journal of Microscopy* 188:264-272

[9] Vicente N.B., Diaz Zamboni J.E., Adur J.F., Izaguirre M.F., Casco V.H. (2008) "Design and validation of an automatic algorithm for deconvolution and quantification in modern microscopy". In *Argentine Symposium on Computing Technology (AST)*

[10] Krotkov E. (1987) "Focusing". *International Journal of Computer Vision* 1:223-237

[11] Adur J., Schlegel J. (1997) "Design, development and construction of an advance micrometric system for microscopes". *Bioengineering Degree Thesis*, Faculty of Engineering – Bioengineering. Entre Ríos National University. Argentina

[12] Diaz-Zamboni J.E., Adur J.F., Fiorucci M.P., Izaguirre F., Casco V.H. (2005) "Algoritmo de desconvolución iterativo con restricción de positividad para imágenes de microscopía de fluorescencia tridimensional". In *XV Congreso Argentino de Bioingeniería*

[13] Diaz-Zamboni J.E. (2004) "Software para usuarios de microscopía de desconvolución digital". *Bioengineering Degree Thesis*, Faculty of Engineering – Bioengineering, Entre Ríos National University, Argentina.

[14] Vicente N.B., Diaz Zamboni J.E., Adur J.F., Paravani E.V., Casco V.H. (2007) "Photobleaching correction in fluorescence microscopy images". *Journal of Physics: Conference Series*, doi: 10.1088/1742-6596/90/1/012068

[15] Benson D.M., Bryan J., Plant A.L., Gotto A.M., Smith L.C. (1985) "Digital imaging fluorescence microscopy: spatial heterogeneity of photobleaching rate constants in individual cells". *The Journal of Cell Biology* 100:1309-1323

[16] Song L., Hennink E.J., Young T., Tanke H.J. (1995) "Photobleaching kinetics of fluorescein in quantitative fluorescence microscopy". *Biophysical Journal* 68:2588-2600

[17] Sibarita J.B. (2005) "Deconvolution microscopy". *Advances in Biochemical Engineering/Biotechnology* 95: 201–243

[18] Gosner K.L. (1960) "A simplified table for stanging anuran embryos and larval with noter on identification". *Herpetologica* 16:183-190

[19] Adams C.L., Chen Y.T., Smith S.J., Nelson W.J. (1998) "Mechanisms of epithelial cell–cell adhesion and cell compaction revealed by high-resolution tracking of E-Cadherin–Green Fluorescent Protein". *The Journal of Cell Biology* 142:1105-1119

[20] Gumbiner B.M. (1996) "Cell adhesion: the molecular basis of tissue architecture and

morphogenesis". *Cell* 84:345-357.

[21] Izaguirre M.F., Adur J.F., Peralta-Soler A., Casco V.H. (2001) "Alterations induced by E-Cadherin and β-catenin antibodies during the development of Bufo arenarum (Anura – Bufonidae)" *Histology and Histopathology* 16:1097-1106

[22] Larrea D., Díaz-Zamboni J.E., Adur J.F., Izaguirre M.F., Casco V.H. (2006) "Expresión tridimensional de cadherina E, alfa- y beta-catenina en la piel, durante el desarrollo de Bufo arenarum". In *IX Jornadas de Ciencias Naturales del Litoral y Reunión Argentina de Ciencias Naturales*. Paraná, Argentina.